

Joint CS-MRI Reconstruction and Segmentation with a Unified Deep Network

Liyan Sun^{*1}, Zhiwen Fan^{*1}, Xinghao Ding(✉)¹, Yue Huang¹, and John Paisley²

¹ Fujian Key Laboratory of Sensing and Computing for Smart City,
Xiamen University, Fujian, China ✉ dxh@xmu.edu.cn

² Department of Electrical Engineering, Columbia University, New York, NY, USA

Abstract. The need for fast acquisition and automatic analysis of MRI data is growing. Although compressed sensing magnetic resonance imaging (CS-MRI) has been studied to accelerate MRI by reducing k-space measurements, current techniques overlook downstream applications such as segmentation when doing image reconstruction. In this paper, we test the utility of CS-MRI when performing automatic segmentation and propose a unified deep neural network architecture called SegNetMRI for simultaneous CS-MRI reconstruction and segmentation. SegNetMRI uses an MRI reconstruction network with multiple cascaded blocks, each containing an encoder-decoder unit and a data fidelity unit, and a parallel MRI segmentation network having the same encoder-decoder structure. The two subnetworks are pre-trained and fine-tuned with shared reconstruction encoders. The outputs are merged into the final segmentation. Our experiments show that SegNetMRI can improve both the reconstruction and segmentation performance when using compressed measurements.

Keywords: compressed sensing · magnetic resonance imaging · medical image segmentation

1 Introduction

Magnetic resonance imaging (MRI) is a fundamental technique for visualizing human tissue. In MRI, raw measurements come in the form of Fourier transform coefficients in “k-space” and the MRI can be viewed after an inverse 2D Fourier transform of the fully sampled k-space. Conventionally, radiologists view MRI for diagnosis. However, in areas where medical expertise may be lacking or not sufficient to meet demand, automated methods may also be useful. To this end, automatic MR image segmentation is essential because it allows for finer localization of focus. To take brain segmentation for example, usually four structures emerge including background, gray matter (GM), white matter (WM) and cerebrospinal fluid (CSF). Lesions appearing in white matter are closely associated with various issues such as strokes and Alzheimer’s disease [25].

Although rich anatomical information can be provided by MRI, it is limited by a long imaging period. This can introduce motion artifacts caused by movement of the

^{*} The co-first authors contributed equally.

patient [3] or induce psychological pressures brought by claustrophobia [11]. Thus accelerating imaging speed while maintaining high imaging quality is key for MRI. Compressed sensing (CS) theory [9, 5], which shows the possibility of recovering signals with sub-Nyquist sampling rates, has been introduced to the field of MRI to accelerate imaging. In 2017, the US Food and Drug Administration (FDA) approved CS-MRI techniques for use by two major MRI vendors: Siemens and GE [10]. Thus, one can expect increasing deployment of CS-MRI technique in the future for real-world applications.

Current segmentation algorithms for MRI assume a “clean” (i.e., fully-sampled) image as input and, to our knowledge, do not take CS-MRI scenarios into consideration. Likewise, CS-MRI reconstruction methods do not consider their output’s potential downstream use for segmentation. Although experienced human experts can make relatively robust decisions with CS-reconstructed images, the anticipated increase in the number of CS-reconstructed MRI for clinical application will call for automatic segmentation algorithms optimized for this type of data. Therefore, a joint approach to MRI reconstruction/segmentation under the compressed sensing framework is worth exploring.

In this paper, we develop a unified deep neural network called SegNetMRI for joint MRI reconstruction and segmentation with compressive measurements. The model is unified in that parameters are ultimately tuned taking both segmentation and reconstruction tasks into consideration. We build SegNetMRI on two joined networks: an MRI reconstruction network (MRN) and MRI segmentation network (MSN). The MSN is an encoder-decoder structure network and for SegNetMRI this is made up of basic blocks which each consist of an encoder-decoder and data fidelity unit. The MRN is pre-trained with pairs of artificially under-sampled MRI and their corresponding fully-sampled MRI, and the MSN is pre-trained with fully-sampled MRI and their corresponding segmentation labels. We then fine-tune the resulting unified network with MSN and MRN both sharing the same encoder component. In this way, the MRI reconstruction and segmentation models can each aid the learning of the other through shared regularization.

2 Background and Related Work

MRI segmentation. Broadly speaking, the research in MRI segmentation can be categorized into three classes: (1) atlas-based segmentation with registration; (2) machine learning models with hand-crafted features; (3) deep learning models. Atlas-based segmentation [1, 2] requires accurate registration and is time-consuming, so it is impractical for applications that require fast speed. In the second class, manually designed features are used for classification, for example 3D Haar/spatial features classified with random forests [27]. Similar to many image processing problems, these hand-crafted features are not very flexible for encoding diverse patterns within the MRI data. Recently deep learning based models have been proposed, such as a 2D convolutional neural network [20, 19], a 3D convolutional neural network [7, 6], and parallelized long short-term memory (LSTM) [26]. These models can learn semantic image features from data, typically leading to the state-of-the-art performance in MRI segmentation. How-

ever, these MRI segmentation models do not take the input quality into consideration, such as degradations from a sub-sampled k-space, but assume a fully-sampled MRI.

Compressed sensing MRI. We briefly review the work in CS-MRI reconstruction. Denote the underlying vectorized MRI $x \in \mathbb{C}^{P \times 1}$, which we seek to reconstruct from the sub-sampled vectorized k-space data $y \in \mathbb{C}^{Q \times 1}$ ($Q \ll P$). CS-MRI inversion is then typically formulated as the optimization

$$x = \arg \min \|F_u x - y\|_2^2 + f_\theta(x), \quad (1)$$

where the $F_u \in \mathbb{C}^{Q \times P}$ denotes the under-sampled Fourier matrix. The ℓ_2 term is the data fidelity and $f_\theta(\cdot)$ represents a regularization with parameter θ to constrain the solution space.

The main research focus of CS-MRI is proposing better f_θ and efficient optimization techniques. In the first CS-MRI work called SparseMRI [17], wavelet domain ℓ_1 sparsity plus image total variation were imposed as regularizations. More complex wavelet variants were designed for CS-MRI in PANO [21] and GBRWT [13]. Dictionary learning techniques have also been introduced to CS-MRI, such as DLMRI [22] and BPTV [12]. These works can all be categorized as sparsity-based CS-MRI methods since they model the MRI with a “one-level” sparse prior. This prior often tends to over-smooth the resulting image.

Recently, deep neural networks have been introduced to CS-MRI. Researchers have directly applied the convolutional neural network (CNN) to learn a direct mapping from the zero-filled MRI $F_u^H y$ (obtained by zero-padding the unsampled positions in k-space) to the true MRI [28]. A deep residual architecture was also proposed for this same mapping [14]. Data fidelity terms have been incorporated into the deep neural network by [24] to add more guidance. These deep learning based CS-MRI models have achieved higher reconstruction quality and faster reconstruction speed.

Combining visual tasks. The combination of different visual tasks into a unified model is frequently considered in the field of computer vision. For example, a joint blind image restoration and recognition model based on sparse coding has been proposed for face recognition with low-quality images [29]. The image dehazing model AOD-Net performs detection in the presence of haze by performing dehazing during detection [15]. In the MRI field, models for 3T-obtained images have been proposed to jointly perform segmentation and super-resolution (7T) image generation [4].

3 Methodology

In this section, we give a detailed description of the proposed SegNetMRI model. First, we propose a segmentation network as baseline and test popular CS-MRI methods with this model. Next we propose an MRI reconstruction network formed by cascading basic network blocks. We show that the proposed MRI reconstruction network achieves better performance on segmentation compared with conventional sparsity-based CS-MRI models, but is still inferior to using the fully-sampled MRI. We finally propose the SegNetMRI model to merge these MRI reconstruction and segmentation approaches into a single model.

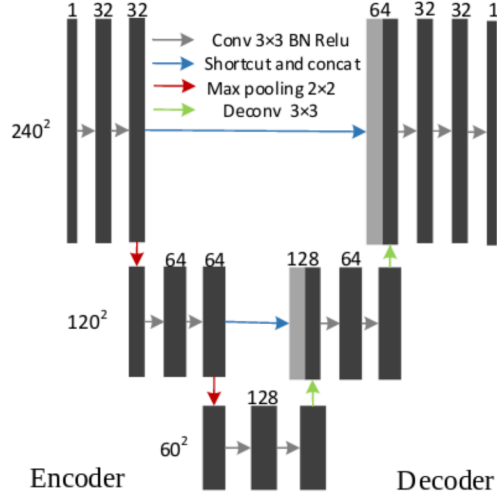


Fig. 1: The MSN architecture composed of an encoder and decoder. We use this segmentation network to compare performance using different CS-MRI reconstruction approaches as input.

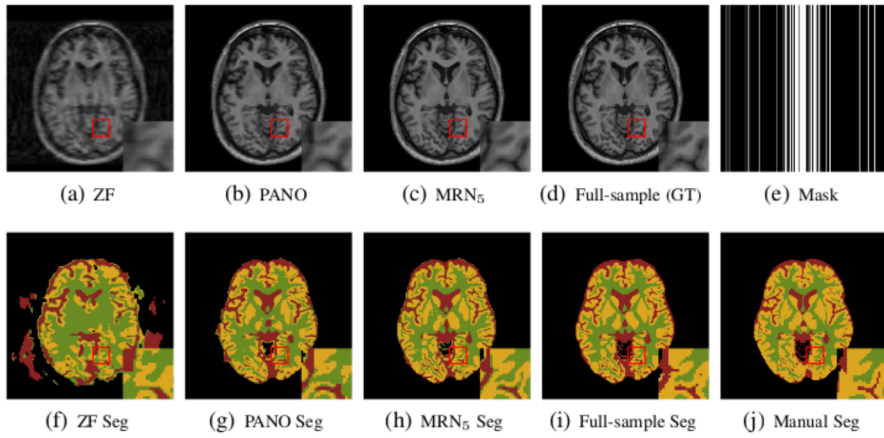


Fig. 2: Top: Reconstructed MRI using different CS-MRI methods and a 20% sampling mask. Bottom: These MRI are segmented using an independently-trained segmentation model based on the state-of-the-art U-Net (referred to as MSN in this paper for its MRI application).

3.1 Illustration: Segmentation after CS-MRI

We first test several popular CS-MRI model outputs on an automatic MRI segmentation model to assess the impact of compressed sensing for the segmentation task. As a basic

segmentation model, we use the MRI segmentation network (MSN) shown in Figure 1, which is the state-of-the-art medical image segmentation model called U-Net [23]. The segmentation encoder (SE) component uses convolution and pooling to extract features from the input image at different scales, and the segmentation decoder (SD) component uses a deconvolution operation to predict the pixel-level segmentation class using these features. Shortcut connections are used by the model to directly send lower-layer feature information to high-layer features by concatenation.

After training this MSN model using fully-sampled MRI and their ground truth segmentation labels, we test model performance using reconstructed MRI produced by various CS-MRI methods. We use a 20% Cartesian under-sampling mask as shown in Figure 2(e). Our tested methods including the degraded zero-filled (ZF) reconstruction as baseline, PANO [21] and the proposed MRN model which will be discussed in the following section. We tuned the parameters of PANO for this problem.

We observe that the zero-filled (ZF) reconstruction in Figure 2(a) produces a low-quality MRI, which leads to the poor segmentation performance shown in Figure 2(f). The PANO reconstructed MRI in Figure 2(b) is segmented better in Figure 2(g), but is still far from satisfactory because of the loss of structural details in the reconstruction. Segmentation using the fully-sampled (FS) MRI in Figure 2(d) is shown in Figure 2(i). Though this isn't the ground truth segmentation, it is the segmentation performed on the ground truth MRI, and so represents an upper bound for CS-MRI on this segmentation task. The manually label segmentation is shown in Figure 2(j). This experiment shows that while CS-MRI can substantially improve the reconstruction quality visually, the fine structural details which are important for segmentation can still be missing, leaving space for improvement.

3.2 An MRI Reconstruction Network

Deep learning for CS-MRI has the advantage of large modeling capacity, fast running speed, and high-level semantic modeling ability, which eases the integration of high-level task information compared with traditional sparsity-based CS-MRI models. Therefore, we adopt the same encoder-decoder architecture in Figure 1 as a basic encoder-decoder unit with a global residual shortcut to reconstruction the sub-sampled MRI. Since information loss can become severe as neural network depth increases, we introduce a data fidelity (DF) unit to help correct the Fourier coefficients of the reconstructed MRI produced by the encoder-decoder architecture on the sampled positions in k-space. This takes advantage of the fact that we have accurate measurements at the under-sampled k-space locations, and so the layers of the network should not override this information. The details of the data fidelity unit can be found in [24].

The encoder-decoder architecture and data fidelity unit make up a basic block. As more blocks are stacked, the quality of the reconstructed MRI at each block gradually improves [24]. We therefore cascade N such basic units to form the MRI reconstruction network (MRN_N) in Figure 3. The reconstruction encoder in different blocks extract features at different depths. Previously in Figure 1, we observed that MRN_5 achieves better reconstruction performance in Figure 2(c) than the non-deep PANO method, but the segmentation output in Figure 2(h) ($\text{MRN} \rightarrow \text{MSN}$) is still inferior to the fully-sampled segmentation. This motivates the following joint learning framework.

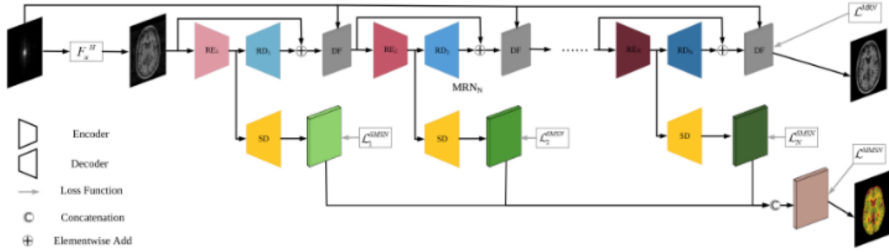


Fig. 3: The SegNetMRI structure, formed by connecting the previously discussed MRN for reconstruction (top) with MSN for segmentation (bottom).

3.3 SegNetMRI: A Unified Deep Neural Network

Using the previously discussed networks as starting points, we design a joint framework for CS-MRI reconstruction/segmentation based on deep learning. We call this joint network SegNetMRI and show its structure in Figure 3. At a high level, the two problems are connected by a shared encoder, while having separate decoders.

To learn this model, we first pre-train two separate models. We pre-train the MRN_N with under-sampled and fully-sampled MRI training pairs. Similarly, we pre-train the MSN with fully-sampled MRI and their corresponding segmentation labels. After training MSN, we discard the encoder component (SE) and keep the decoder component (SD). We then connect the single decoder component of the MSN (SD) to each of the encoder components of each MRN (called RE_n) within each block. The resulting N outputs of the MSN decoder for each block are concatenated and merged to give the final segmentation via a 1×1 convolution. After pre-training separately and initializing the remaining parts, the parameters of SegNetMRI_N (with N blocks in the MRN portion, but a single segmentation decoder duplicated N times) are then fine-tuned. Therefore, both the reconstruction and segmentation tasks share the *same* encoders, but have *separate* decoders for their respective tasks.

The rationale for using this architecture is as follows:

1. With the pre-training of MRN_N , the reconstruction encoder extracts basic features in different blocks. In SegNetMRI, the sharing of the reconstruction encoders between MRN and MSN means that these same features are used for both reconstruction and segmentation. This can help the two problems regularize each other.
2. The segmentation component uses information at various depths in the cascaded MRN and combines this information in the decoder. The 1×1 convolution used to merge the outputs of the segmentation decoder at each layer can be viewed as ensemble learning.

Loss function. We use Euclidean distance as the loss function for pre-training MRN,

$$\mathcal{L}^{\text{MRN}} = \frac{1}{L} \sum_{i=1}^L \|x_i^{fs} - x_i\|_2^2, \quad (2)$$

where x_i^{fs} and x_i are the i^{th} fully-sampled training image and the output of MRN, respectively. To pre-train MSN, we use the pixel-wise cross-entropy loss function

$$\mathcal{L}^{\text{MSN}} = - \sum_{i=1}^L \sum_{j=1}^N \sum_{c=1}^C t_{ijc}^{gt} \ln t_{ijc}, \quad (3)$$

where C tissue classes are to be classified. t^{gt} and t is the pixel-wise ground-truth label and the MSN-predicted label, respectively.

After pre-training MRN and MSN, we then construct and fine-tune SegNetMRI using the following loss function

$$\mathcal{L}^{\text{SegNetMRI}} = \mathcal{L}^{\text{MRN}} + \lambda \mathcal{L}^{\text{OMSN}}. \quad (4)$$

We set $\lambda = 0.01$ in our experiments. The overall MSN (OMSN) loss, consisting of $N + 1$ loss function terms if SegNetMRI contains N blocks, is

$$\mathcal{L}^{\text{OMSN}} = \frac{1}{N+1} \left(\mathcal{L}^{\text{MMSN}} + \sum_{i=1}^N \mathcal{L}_i^{\text{SMSN}} \right), \quad (5)$$

where the $\mathcal{L}^{\text{MMSN}}$ is the loss for the merged prediction and $\mathcal{L}_i^{\text{SMSN}}$ is the loss for each sub-MSN decoder prediction.

4 Experiments and Discussions

4.1 Implementation Details

Setup. We implement all deep models on TensorFlow for the Python environment using a NVIDIA Geforce GTX 1080Ti with 11GB GPU memory and Intel Xeon CPU E5-2683 at 2.00GHz. We show the hyperparameter settings of encoder-decoder architecture used for both MRN and MSN in Figure 1. We use batch normalization to stabilize training. ReLU is used as the activation function, except for the last convolutional layer of the encoder-decoder unit within each MRN block, where the identity map is applied for residual learning. We apply Xavier initialization for pre-training MRN and MSN. MSN is pre-trained for 60,000 iterations using 64×64 fully-sampled MRI patches randomly cropped (16 patches in a batch) and MRN is pre-trained for 30,000 iterations using the entire training image (4 images in a batch). We then fine-tune the SegNetMRI model for 8,000 further iterations using entire images (4 images in a batch). ADAM is chosen as optimizer. We select the initial learning rate to be 0.0005, the first-order momentum to be 0.9 and the second momentum to be 0.999.

Data. We test SegNetMRI on the MRBrainS datasets from the Grand Challenge on MR Brain Image Segmentation (MRBrainS) Workshop [18]. These datasets are acquired using 3T MRI scans. Five datasets are provided containing T1-1mm, T1, T1-IR and T2-FLAIR imaging modalities already registered and with manual segmentations. Here we use the T1 MRI data of the size 240×240 throughout the paper. We use four datasets for training (total 192 slices) and one dataset for testing (total 48 slices). We adopt the same data augmentation technique discussed in [8].

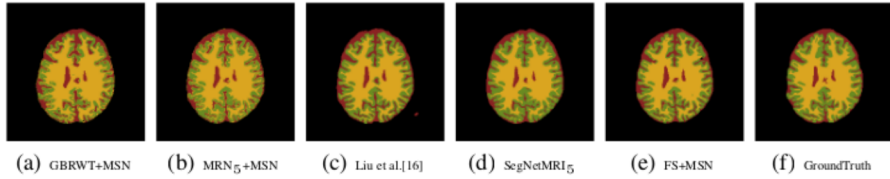


Fig. 4: The segmentations of the compared methods.

Methods	GM			WM			CSF		
	DC	HD	AVD	DC	HD	AVD	DC	HD	AVD
GBRWT+MSN	75.55	2.24	4.21	65.56	1.90	3.10	76.50	1.77	2.69
MRN ₅ +MSN	79.36	2.06	3.57	65.76	1.88	2.96	78.43	1.64	2.33
Liu et al. [16]	83.41	1.81	2.96	78.05	1.24	1.61	77.81	1.76	2.58
SegNetMRI ₅	86.38	1.66	2.52	81.49	1.08	1.34	79.23	1.61	2.23
FS+MSN	87.36	1.60	2.33	85.94	1.00	1.14	81.01	1.61	2.18

Table 1: The segmentation performance of different models using DC (%), HD and AVD (%) as metrics. FS+MSN is the segmentation performance when the ground truth MRI is known. We consider FS+MSN the upper bound on performance given our chosen MSN approach.

4.2 Experimental Results

To evaluate the segmentation performance, we compare the proposed SegNetMRI₅ (5 blocks) with the following: 1) inputting a fully-sampled MRI into MSN (FS+MSN), which we take as ground truth performance; 2) inputting the MRN₅ reconstruction into MSN (MRN₅+MSN), i.e., no joint learning; 3) inputting the GBRWT model reconstruction into MSN (GBRWT+MSN), since GBRWT [13] represents the state-of-the-art performance among non-deep sparsity-based CS-MRI methods; 4) finally, we also compare with the joint framework proposed by [16], where only the reconstruction network is fine-tuned in MRN₅+MSN using the loss function $\mathcal{L}^{\text{MRN}} + \lambda \mathcal{L}^{\text{MSN}}$. The same under-sampling mask shown in Figure 2(e) is again used.

We show a qualitative performance comparison in Figure 4. We color the segmentation corresponding to white matter (yellow), gray matter (green) and cerebrospinal fluid (yellow). We observe that the proposed SegNetMRI₅ model provides better segmentation and approximates the ideal FS+MSN most closely, both of which are not perfect compared with the human labeling. For quantitative evaluation, we use the Dice Coefficient (DC), the 95th-percentile of the Hausdorff distance (HD) and the absolute volume difference (AVD), which are also used in the MRBrainS challenge [18]. Larger DC and smaller HD and AVD indicate better segmentation. We show these results in Table 1, which is consistent with our subjective evaluation.

In addition to the improved segmentation accuracy, we also evaluate the reconstruction quality of SegNetMRI. We show the reconstructed MRI from SegNetMRI₅, the

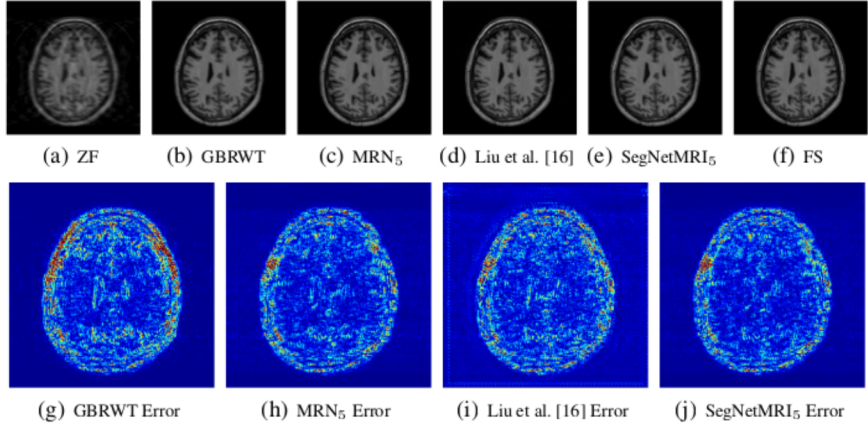


Fig. 5: (top) reconstructed MRI using various methods (top). (bottom) approximation residuals.

	GBRWT	MRN ₅	Liu et al.[16]	SegNetMRI ₅
PSNR	31.80	33.94	33.47	34.27
NMSE	0.0584	0.0361	0.0388	0.0333

Table 2: The averaged PSNR (dB) and NMSE on 37 test MRI.

joint framework from [16], MRN₅ and GBRWT in Figure 5, along with their corresponding residuals. (We set the error ranges from [0 0.1] on a [0 1] pre-scaled image.) We find that SegNetMRI achieves the minimal reconstruction error, especially in the meaningful tissue regions. We also give averaged reconstruction performance measures in Table 2 using peak signal-to-noise ratio (PSNR) and the corresponding normalized mean squared error (NMSE) on all 37 test MRI. We see that the segmentation information is able to aid learning the reconstruction network as well.

Discussion. It is worth noting that the the model in [16] achieves better segmentation performance than an independently learned MRN₅ model (i.e., no joint learning), but that reconstruction quality is worse than MRN₅ both qualitatively and quantitatively. The original work in [16] is devoted to joint natural image denoising and segmentation, with segmentation taking priority. However, for the medical image analysis problem the reconstruction and segmentation performance are both important; often a radiologists will hand-segment for diagnosis, which is made more difficult by poor reconstruction. Therefore, SegNetMRI has been designed to equally weight the performance on both reconstruction and segmentation in model learning.

In SegNetMRI_N, the output of N MSN decoders are concatenated and merged into the final segmentation using a 1×1 convolution. This ensemble learning can make full use of the information from different depths of SegNetMRI and so produce better segmentation accuracy. To illustrate, we consider the SegNetMRI₅ result on the gray

GM	B ₁	B ₂	B ₃	B ₄	B ₅	Merged
DC	75.15	80.31	83.64	81.02	85.66	86.38
HD	2.15	1.95	1.77	1.90	1.68	1.66
AVD	4.35	3.58	2.90	3.43	2.60	2.52

Table 3: We compare the segmentation performance of the outputs from each block in SegNetMRI₅ model without using 1×1 convolution to fuse their information. SegNetMRI₅ does this fusion.

matter tissue of all test MRI. In Table 3, we show the segmentation performance of the outputs from each block in SegNetMRI₅ model without the 1×1 convolution, and we compare them with the segmentation output produced after merging the SegNetMRI₅ outputs using 1×1 convolution. It is clear that the output of SegNetMRI₅ can achieve better segmentation performance by fusing the outputs from all layers, even though individual performance is worse at shallower layers.

In Figure 6, we show the segmentation accuracy as a function of number of blocks N using the Dice Coefficient metric. The reconstruction quality (in PSNR) improves as the number of the blocks increases in SegNetMRI, but at the expense of longer training time.

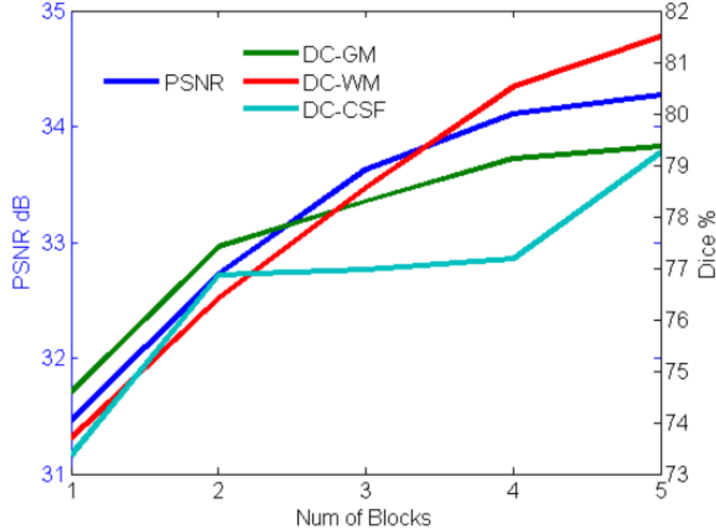


Fig. 6: The model performance of SegNetMRI_N as a function of the number of blocks.

5 Conclusion

Automatic segmentation of MRI is an important problem in medical imaging, and with the recent adoption of CS-MRI by industry, segmentation techniques that take CS-MRI reconstruction into account are needed. After verifying that the two tasks suffer when done independently, we proposed a deep neural network architecture called SegNetMRI to merge the MRI reconstruction and segmentation problems into a joint framework. Our experiments show that doing simultaneous reconstruction and segmentation can positively reinforce each other, improving both tasks significantly.

Acknowledgements

This work was supported in part by the National Natural Science Foundation of China under Grants 61571382, 81671766, 61571005, 81671674, 61671309 and U1605252, in part by the Fundamental Research Funds for the Central Universities under Grant 20720160075, 20720180059, in part by the CCF-Tencent open fund and, the Natural Science Foundation of Fujian Province of China (No. 2017J01126). L. Sun conducted portions of this work at Columbia University under China Scholarship Council grant No. 201806310090.

References

1. Aljabar, P., Heckemann, R.A., Hammers, A., Hajnal, J.V., Rueckert, D.: Multi-atlas based segmentation of brain images: atlas selection and its effect on accuracy. *Neuroimage* **46**(3), 726–738 (2009)
2. Artaechevarria, X., Munoz-Barrutia, A., Ortiz-de Solórzano, C.: Combination strategies in multi-atlas image segmentation: Application to brain MR data. *IEEE Trans. on Medical Imaging* **28**(8), 1266–1277 (2009)
3. Atkinson, D., Hill, D.L., Stoyle, P.N., Summers, P.E., Clare, S., Bowtell, R., Keevil, S.F.: Automatic compensation of motion artifacts in MRI. *Magnetic Resonance in Medicine* **41**(1), 163–170 (1999)
4. Bahrami, K., Rekik, I., Shi, F., Shen, D.: Joint reconstruction and segmentation of 7t-like mr images from 3t mri based on cascaded convolutional neural networks. In: MICCAI. pp. 764–772. Springer (2017)
5. Candès, E.J., Romberg, J., Tao, T.: Robust uncertainty principles: Exact signal reconstruction from highly incomplete frequency information. *IEEE Trans. on Information Theory* **52**(2), 489–509 (2006)
6. Chen, H., Dou, Q., Yu, L., Qin, J., Heng, P.A.: Voxresnet: Deep voxelwise residual networks for brain segmentation from 3D MR images. *NeuroImage* (2017)
7. Çiçek, Ö., Abdulkadir, A., Lienkamp, S.S., Brox, T., Ronneberger, O.: 3D U-Net: learning dense volumetric segmentation from sparse annotation. In: MICCAI. pp. 424–432. Springer (2016)
8. Dong, H., Yang, G., Liu, F., Mo, Y., Guo, Y.: Automatic brain tumor detection and segmentation using u-net based fully convolutional networks. In: Annual Conference on Medical Image Understanding and Analysis. pp. 506–517. Springer (2017)
9. Donoho, D.L.: Compressed sensing. *IEEE Trans. on Information Theory* **52**(4), 1289–1306 (2006)

10. Fessler, J.A.: Medical image reconstruction: a brief overview of past milestones and future directions. arXiv preprint arXiv:1707.05927 (2017)
11. Hricak, H., Amparo, E.: Body MRI: alleviation of claustrophobia by prone positioning. *Radiology* **152**(3), 819–819 (1984)
12. Huang, Y., Paisley, J., Lin, Q., Ding, X., Fu, X., Zhang, X.P.: Bayesian nonparametric dictionary learning for compressed sensing MRI. *IEEE Trans. on Image Processing* **23**(12), 5007–5019 (2014)
13. Lai, Z., Qu, X., Liu, Y., Guo, D., Ye, J., Zhan, Z., Chen, Z.: Image reconstruction of compressed sensing MRI using graph-based redundant wavelet transform. *Medical Image Analysis* **27**, 93–104 (2016)
14. Lee, D., Yoo, J., Ye, J.C.: Deep residual learning for compressed sensing MRI. In: ISBI. pp. 15–18. IEEE (2017)
15. Li, B., Peng, X., Wang, Z., Xu, J., Feng, D.: Aod-net: All-in-one dehazing network. In: ICCV (Oct 2017)
16. Liu, D., Wen, B., Liu, X., Wang, Z., Huang, T.S.: When image denoising meets high-level vision tasks: A deep learning approach. In: IJCAI (2018)
17. Lustig, M., Donoho, D., Pauly, J.M.: Sparse MRI: The application of compressed sensing for rapid MR imaging. *Magnetic Resonance in Medicine* **58**(6), 1182–1195 (2007)
18. Mendrik, A.M., Vincken, K.L., Kuijf, H.J., Breeuwer, M., Bouvy, W.H., De Bresser, J., Alansary, A., De Bruijne, M., Carass, A., El-Baz, A., et al.: MRBrainS challenge: online evaluation framework for brain image segmentation in 3T MRI scans. *Computational Intelligence and Neuroscience* **2015**, 1 (2015)
19. Moeskops, P., Viergever, M.A., Mendrik, A.M., de Vries, L.S., Benders, M.J., Išgum, I.: Automatic segmentation of MR brain images with a convolutional neural network. *IEEE Trans. on Medical Imaging* **35**(5), 1252–1261 (2016)
20. Nie, D., Wang, L., Gao, Y., Sken, D.: Fully convolutional networks for multi-modality iso-intense infant brain image segmentation. In: ISBI. pp. 1342–1345. IEEE (2016)
21. Qu, X., Hou, Y., Lam, F., Guo, D., Zhong, J., Chen, Z.: Magnetic resonance image reconstruction from undersampled measurements using a patch-based nonlocal operator. *Medical Image Analysis* **18**(6), 843–856 (2014)
22. Ravishankar, S., Bresler, Y.: MR image reconstruction from highly undersampled k-space data by dictionary learning. *IEEE Trans. on Medical Imaging* **30**(5), 1028–1041 (2011)
23. Ronneberger, O., Fischer, P., Brox, T.: U-net: Convolutional networks for biomedical image segmentation. In: MICCAI. pp. 234–241. Springer (2015)
24. Schlemper, J., Caballero, J., Hajnal, J.V., Price, A., Rueckert, D.: A deep cascade of convolutional neural networks for MR image reconstruction. In: IPMI. pp. 647–658. Springer (2017)
25. Steenwijk, M.D., Pouwels, P.J., Daams, M., van Dalen, J.W., Caan, M.W., Richard, E., Barkhof, F., Vrenken, H.: Accurate white matter lesion segmentation by k nearest neighbor classification with tissue type priors (kNN-TTPs). *NeuroImage: Clinical* **3**, 462–469 (2013)
26. Stollenga, M.F., Byeon, W., Liwicki, M., Schmidhuber, J.: Parallel multi-dimensional lstm, with application to fast biomedical volumetric image segmentation. In: NIPS. pp. 2998–3006 (2015)
27. Wang, L., Gao, Y., Shi, F., Li, G., Gilmore, J.H., Lin, W., Shen, D.: Links: Learning-based multi-source integration framework for segmentation of infant brain images. *NeuroImage* **108**, 160–172 (2015)
28. Wang, S., Su, Z., Ying, L., Peng, X., Zhu, S., Liang, F., Feng, D., Liang, D.: Accelerating magnetic resonance imaging via deep learning. In: ISBI. pp. 514–517. IEEE (2016)
29. Zhang, H., Yang, J., Zhang, Y., Nasrabadi, N.M., Huang, T.S.: Close the loop: Joint blind image restoration and recognition with sparse representation prior. In: ICCV. pp. 770–777. IEEE (2011)